Path Descriptors for Geometric Graph Matching and Registration

Miguel Amável Pinheiro and Jan Kybic

Center for Machine Perception, Dept. of Cybernetics, Faculty of Electrical Engineering, Czech Technical University in Prague, Czech Republic

Abstract. Graph and tree-like structures such as blood vessels and neuronal networks are abundant in medical imaging. We present a method to calculate path descriptors in geometrical graphs, so that the similarity between paths in the graphs can be determined efficiently. We show experimentally that our descriptors are more discriminative than existing alternatives. We further describe how to match two geometric graphs using our path descriptors. Our main application is registering images for which standard techniques are inefficient, because the appearance of the images is too different, or there is not enough texture and no uniquely identifiable keypoints to be found. We show that our approach can register these images with better accuracy than previous methods.

1 Introduction

Blood vessels, nerve fibers or pulmonary airways are examples of biological structures that can be represented as *geometrical graphs* with nodes corresponding to branching points and edges corresponding to curves connecting the branching points (Fig. 1). We consider the problem of registering two 2D or 3D images based on a common geometric graph structure both images contain and which we assume to be already extracted (e.g. [1]). This approach has the potential of being much faster than standard pixel-based image registration techniques [2] and tolerate very different image appearances. With respect to key point registration methods [3], registering geometric graphs provides more clues.

Unlike most existing approaches, our method can in a reasonable time handle rather general transformations and large displacements, as well as partial overlaps. The key contribution over our previous work [4, 5] is an alternative coarse alignment step based on finding similarities between *path descriptors* to restrict the set of possible correspondences and thus make the matching more efficient.

2 Related work

Ignoring edges, the geometric graph registration becomes a point cloud matching problem, which can be solved by RANSAC-like approaches [6, 7] These methods do not need initialization but only work for restricted class of transformations, such as rigid or affine. On the other hand ICP-like approaches [8, 9] can handle

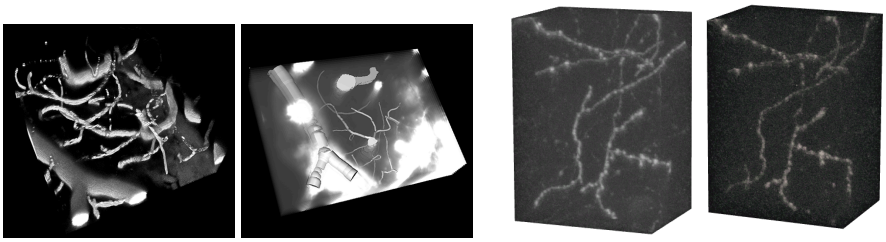

(a) (b) (c) (d)

Fig. 1. Example registration problems with prominent geometric graph structures: Blood vessels in brain tissue acquired using **(a)** two photon microscopy and **(b)** bright-field optical microscopy; two-photon microscopy images of axons in the brain **(c,d)**.

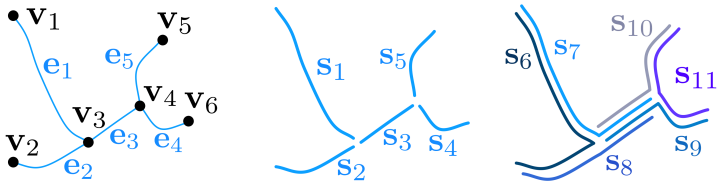

Fig. 2. Example of the representation and notation for a graph with $K = 2$.

nonlinear transformations but require a good initialization. Finally, the matching can be viewed as a discrete optimization problem with cost functions assigned to node or edge pairings [10–12], which is very powerful but computationally demanding. Pruning the search space is important to increase efficiency [4, 5] and node and edge descriptors [13, 14] can be used for that purpose.

3 Problem definition

Let us have an undirected graph $\mathbf{G}^A = (\mathbf{V}^A, \mathbf{E}^A)$ with nodes $\mathbf{V}^A = \{\mathbf{v}_1^A, \ldots, \mathbf{v}_{|\mathbf{V}^A|}^A\}$ and edges $\mathbf{E}^A = \{e_1^A, \ldots, e_{|\mathbf{E}^A|}^A\}$. We represent each edge $\mathbf{e}_k^A \in \mathbf{E}^A$ as a cubic B-spline [15], limiting the generality of the representable shapes in exchange to better robustness with respect to noise. In doing so, we now have a continuous representation of each edge, which can be represented by a mapping $\xi_{\mathbf{e}_k^A} : [0,1] \to \mathbb{R}^D$, where if $\mathbf{e}_k^A = (\mathbf{v}_i^A, \mathbf{v}_j^A)$, then $\xi_{\mathbf{e}_k^A}(0) = \mathbf{v}_i^A$ and $\xi_{\mathbf{e}_k^A}(1) = \mathbf{v}_j^A$.

We define *superedges* $\mathbf{S}^A$ of graph $\mathbf{G}^A$ as paths of at most K consecutive edges. Similarly to edges, we can now define a mapping $\xi_{\mathbf{s}_k^A} : [0,1] \to \mathbb{R}^D$, which will define the path of each superedge. Superedges are needed to deal with the case of approximative matching, where some nodes and edges are detected only in one of the graphs. Our graph can then be represented by $\mathcal{G}^A = (\mathbf{V}^A, \mathbf{S}^A)$, i.e. a set of nodes and a set of superedges.

Let us now introduce a second graph $\mathcal{G}^B = (\mathbf{V}^B, \mathbf{S}^B)$, which is related to $\mathcal{G}^A$ by a matching $\mathcal{M}_{A\to B} = (M_\mathbf{V}, M_\mathbf{S}, T)$, where $M_\mathbf{V} : \mathbf{V} \to \mathbf{V}$ is a mapping between nodes and $M_\mathbf{S} : \mathbf{S} \to \mathbf{S}$ is a mapping between superedges. The transformation T provides us a mapping of both $\mathbf{V}^A$ and $\mathbf{S}^A$ to $\mathbf{V}^B$ and $\mathbf{S}^B$ respectively,

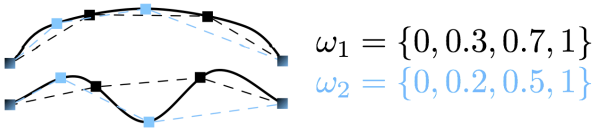

Fig. 3. Example of sampling vectors on two curves.

in $\mathbb{R}^D$. The elements of $\mathcal{M}_{A\to B}$ are not independent. In fact, if one of them is given, it is possible to at least approximate the remaining two. The task is therefore to find $\mathcal{M}_{A\to B}$. We will solve this task by finding similarities between the superedges $\mathbf{S}^A$ and $\mathbf{S}^B$, using path descriptors to be defined in Section 4.

4 Path descriptors

The geometrical transformation between images in biomedical applications can usually be decomposed into a rigid motion plus a mildly non-linear component. Typically, the scale is known from the acquisition parameters and we can consider it is equal to zero, without loss of generality. Due to mechanical properties of the tissue, the nonlinear component is small and we therefore assume that for all $\mathbf{x}, \mathbf{y} \in \mathbb{R}^D$, there is a bound ε_T on the relative length change, such that

$$\frac{1}{1+\varepsilon_T} d\big(\mathbf{x}, \mathbf{y}\big) \leq d\big(T(\mathbf{x}), T(\mathbf{y})\big) \leq (1+\varepsilon_T) d\big(\mathbf{x}, \mathbf{y}\big), \tag{1}$$

holds for a transformation T, where $d(\mathbf{x}, \mathbf{y})$ is the Euclidean distance and ε_T is a *deformation parameter*, i.e. it is bi-Lipschitz.

We propose to use *path descriptors* – a vector characterizing each curve associated with a geometric graph edge. Unlike previously suggested curve descriptors [13, 14, 16], we have a good estimate of the change of descriptor values under our transformation model. Let us have a *sampling vector* $\boldsymbol{\omega} = (\omega_0, \ldots, \omega_{n_\omega+1})$, such that $0 = \omega_0 < \omega_1 < \cdots < \omega_{n_\omega} < \omega_{n_\omega+1} = 1$. Given a geometric path $\xi_{\mathbf{s}_k} \colon [0,1] \to \mathbb{R}^d$ (Section 3) of a superedge $\mathbf{s}_k$, we calculate its descriptor parameterized by $\boldsymbol{\omega}$:

$$h_{\boldsymbol{\omega}}(\mathbf{s}_k) = \sum_{i=0}^{n_\omega} d\big(\xi_{\mathbf{s}_k}(\omega_i), \xi_{\mathbf{s}_k}(\omega_{i+1})\big) = \sum_{i=0}^{n_\omega} \|\xi_{\mathbf{s}_k}(\omega_{i+1}) - \xi_{\mathbf{s}_k}(\omega_i)\|. \tag{2}$$

In plain words, we resample the path in $n_\omega + 2$ points, pass a piecewise linear approximation through the points and calculate the length of this approximation. For an allowable transformation (1), we assume that

$$\frac{1}{1+\varepsilon_h} h_{\boldsymbol{\omega}}(\mathbf{s}_k) \leq h_{\boldsymbol{\omega}}\big(T(\mathbf{s}_k)\big) \leq (1+\varepsilon_h) h_{\boldsymbol{\omega}}(\mathbf{s}_k), \tag{3}$$

for an ε_h close to ε_T. This holds as long as the transformation T is not too far from a rigid body transformation. Given a set of sampling vectors $\boldsymbol{\Omega} = (\boldsymbol{\omega}_1, \ldots, \boldsymbol{\omega}_{|\boldsymbol{\Omega}|})$, we can calculate a vector of descriptors $\mathbf{h}_{\boldsymbol{\Omega}}(\mathbf{s}_k) = \big(h_{\boldsymbol{\omega}_1}(\mathbf{s}_k), \ldots,$

$h_{\boldsymbol{\omega}_{|\boldsymbol{\Omega}|}}(\mathbf{s}_k)\big)$. Given a large enough size of $\boldsymbol{\Omega}$, the value of the vector $\mathbf{h}_{\boldsymbol{\Omega}}(\mathbf{s}_k)$ will describe the geometric disposition of the superedge in $\mathbb{R}^D$.

Given two geometric graphs $\mathcal{G}^A = (\mathbf{V}^A, \mathbf{S}^A)$ and $\mathcal{G}^B = (\mathbf{V}^B, \mathbf{S}^B)$, we say that two superedges $\mathbf{s}_k^A \in \mathbf{S}^A$ and $\mathbf{s}_l^B \in \mathbf{S}^B$ are *compatible* with respect to $\mathbf{h}_{\boldsymbol{\Omega}}$, if (3) holds for all $\boldsymbol{\omega} \in \boldsymbol{\Omega}$,

$$\frac{1}{1+\varepsilon_h}\mathbf{h}_{\boldsymbol{\Omega}}(\mathbf{s}_k^A) \leq \mathbf{h}_{\boldsymbol{\Omega}}\big(\mathbf{s}_l^B\big) \leq (1+\varepsilon_h)\mathbf{h}_{\boldsymbol{\Omega}}(\mathbf{s}_k^A), \tag{4}$$

where the multiplication and comparison is done element by element.

5 Finding a global solution

To find a solution based on our descriptors we formalize our problem as an integer quadratic program (IQP) [10, 17]. Given the graphs $\mathcal{G}^A = (\mathbf{V}^A, \mathbf{S}^A)$ and $\mathcal{G}^B = (\mathbf{V}^B, \mathbf{S}^B)$ we define an affinity matrix $\mathbf{W}$ with size $|\mathbf{V}^A|\cdot|\mathbf{V}^B| \times |\mathbf{V}^A|\cdot|\mathbf{V}^B|$ and elements $W_{ik;jl} = \exp(-||\mathbf{h}_{\Omega}(\mathbf{s}_a^A) - \mathbf{h}_{\boldsymbol{\Omega}}(\mathbf{s}_b^B)||/\sigma^2)$ similarly as in [10, 17], if $\mathbf{s}_a^A = (\mathbf{v}_i^A, \mathbf{v}_j^A) \in \mathbf{S}^A, \mathbf{s}_b^B = (\mathbf{v}_k^B, \mathbf{v}_l^B) \in \mathbf{S}^B$ and the superedge pair $(\mathbf{s}_a^A, \mathbf{s}_b^B)$ is compatible, i.e. if eq. (4) holds. Otherwise $W_{ik;jl} = 0$. If matching node $\mathbf{v}_i^A$ with $\mathbf{v}_k^B$ is consistent with matching node $\mathbf{v}_j^A$ with $\mathbf{v}_l^B$, $W_{ik;jl}$ is high and vice versa.

The matching is represented by a binary vector $\mathbf{x}^*$, such that $\mathbf{x}_{ij} = 1$ iff nodes $\mathbf{v}_i^A$ and $\mathbf{v}_j^B$ match, maximizing the total affinity

$$\mathbf{x}^* = \arg\max_{\mathbf{x}} \mathbf{x}^\intercal \mathbf{W} \mathbf{x} \quad \text{s.t.} \quad \mathbf{x} \in [0,1]^{|\mathbf{V}^A||\mathbf{V}^B|}, \tag{5}$$
$$\forall j \sum_{i=1}^{|U|} \mathbf{x}_{ij} \leq 1, \quad \forall i \sum_{j=1}^{|V|} \mathbf{x}_{ij} \leq 1.$$

Furthermore, there are constraints on node positions:

$$\forall \mathbf{x}_{ik}, \mathbf{x}_{jl} \neq 0, \quad \frac{1}{1+\varepsilon_T}||\mathbf{v}_i^A - \mathbf{v}_j^A|| \leq ||\mathbf{v}_k^B - \mathbf{v}_l^B|| \leq (1+\varepsilon_T)||\mathbf{v}_i^A - \mathbf{v}_j^A||. \tag{6}$$

We use the Reweighted Random Walks method [17] to find an approximate solution $\tilde{\mathbf{x}}^*$ of this NP-hard problem [18]. In order to find the required binary vector $\mathbf{x}^*$, we use the Hungarian algorithm [19] to calculate the best assignment using the weights of $\tilde{\mathbf{x}}^*$. We iteratively select the best individual assignment which does not contradict the previously selected ones and also (6).

This may give us a partial mapping $M_{\mathbf{V}}$, with only a subset of the nodes matched. In order to complete and refine $M_{\mathbf{V}}$ and also to match the paths between nodes, we use a fine alignment algorithm described in [5]. This technique first uses $M_{\mathbf{V}}$ to predict the elastic transformation T represented by a Gaussian process model. Given T, it then uses the Hungarian algorithm to calculate the optimal matching $M_{\mathbf{V}}$ between nodes as well as the matching between other points on the edges, repeating until convergence.

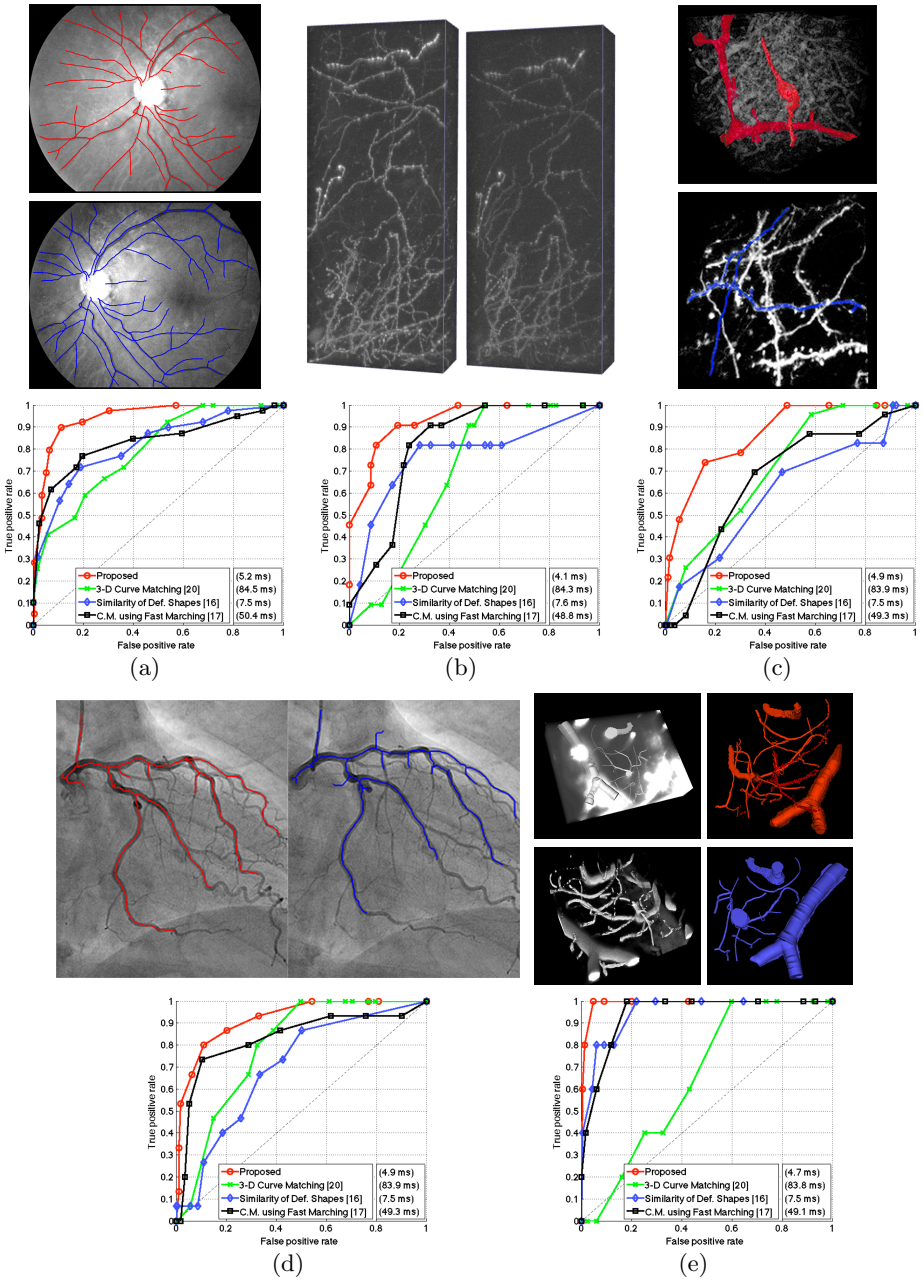

Fig. 4. ROC curve of the performance and average processing times for each of the descriptors in **(a)** retinal fundus [20], **(b)** 2-photon microscopy of neuronal network [21], **(c)** electron (top) and light (bottom) microscopy of neuronal network, **(d)** angiography and **(e)** optical (top) and 2-photon (bottom) microscopy of brain blood vessels.

6 Experiments and results

6.1 Datasets

We test our path descriptors and global matching with datasets from various applications in medical imaging, featuring graph-like structures to be registered. In retinal fundus imaging (see Fig. 4(a)), the registration of different frames taken from various views helps build a single view of the retinal fundus [20].

In neuroscience, to better understand the learning of cognitive functions, images in vivo of the axons in the brain of a mouse are acquired before and after a learning task using 2-photon microscopy [21]. Due to the complexity and small (but crucial) changes in the images (see Fig. 4(b)), the registration procedure helps identifying the differences between the structures. The registration of images acquired with different modalities such as electron and light microscopy (see Fig. 4(c)) is helpful to have a better understanding of the neuronal network [12].

In angiography (see Fig. 4(d)), image registration helps tracking the displacement of the blood vessels in the heart, during heart cycle. The registration of images of blood vessels in the brain acquired using different imaging techniques, such as optical and 2-photon microscopy (see Fig. 4(e)) helps find details which are present in only one of the acquisition techniques [4].

6.2 Path descriptors

To validate the path descriptors, we take two graphs, $\mathcal{G}^A = (\mathbf{V}^A, \mathbf{S}^A)$ and $\mathcal{G}^B = (\mathbf{V}^B, \mathbf{S}^B)$ and calculate the path descriptors $\mathbf{h}_{\mathbf{\Omega}}$ for all superedges in both graphs. For each pair of superedges $\mathbf{s}_k^A \in \mathbf{S}^A$ and $\mathbf{s}_l^B \in \mathbf{S}^B$ we determine if they are compatible (eq. (4)) with respect to $\mathbf{h}_{\mathbf{\Omega}}$ for different ε_h.

In Fig. 4, we show the ROC curves for various previously described datasets. To obtain the ground truth, we assume a superedge $\mathbf{s}_k^A$ is a true match of $\mathbf{s}_l^B$ if both their end nodes match. Apart from the proposed path descriptor, we tested 3-D Curve Matching [16], Determining the Similarity of Deformable Shapes [13], and Curve Matching using Fast Marching [14]. We have varied ε_h for the proposed method, the deformation cost for [13, 14] and the residual Euclidean distance between the matched curves for [16]. Clearly, the proposed descriptor obtains the best performance in all tested datasets.

6.3 Global matching

We used the methodology described in Sec. 5 to find the match $\mathcal{M}$ between the given graphs $\mathcal{G}^A$ and $\mathcal{G}^B$. In Fig. 5, we depict the results of applying this final alignment, based on the proposed path descriptors.

In Table 1, we show the average Euclidean distance between true matches of the registered graphs and the respective processing times using different approaches, namely CPD [9], IPFP [10] and ATS [5], with recommended parameters. In most cases, our proposed method presents the smallest error of all tested methods. The average error is close to the performance of ATS, however accomplished in a much faster time.

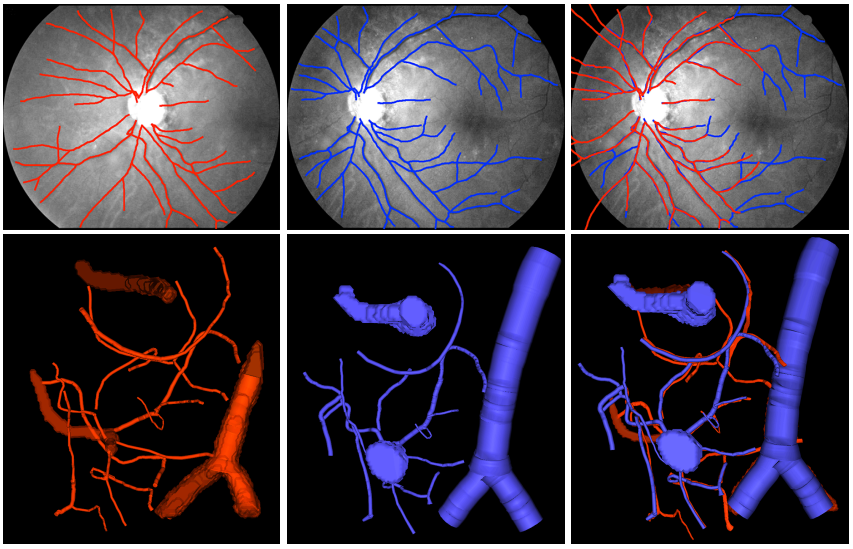

(a) (b) (c)

Fig. 5. Registration results. **(a)** and **(b)** are the original images or structures. **(c)** is the obtained alignment with the proposed approach.

Datasets	**Proposed**	**CPD**[9]	**IPFP**[10]	**ATS**[5]
Retina (Fig. 4(a))	**0.012** / 173.7	0.327 / 6.0	0.540 / 7.0	0.015 / 1155.8
Axons (Fig. 4(b))	**0.013** / 106.5	0.014 / 17.4	0.770 / 57.0	0.087 / 4172.5
EM/LM (Fig. 4(c))	0.053 / 12.8	0.449 / 0.2	0.191 / 0.2	**0.035** / 49.2
Angiography (Fig. 4(d))	**0.024** / 12.6	0.065 / 0.8	0.067 / 0.4	0.026 / 308.7
Brain vessels (Fig. 4(e))	**0.028** / 18.6	0.108 / 1.4	0.542 / 0.6	0.052 / 615.7

Table 1. Average distance between true matches of registered graphs and processing times in seconds separated by a backslash for proposed approach and other methods. Graphs were normalized s. t. $\mathbf{V}^A, \mathbf{V}^B \in [-1, 1]^D$.

7 Conclusion

We presented an approach for matching geometric tree-like structures using path descriptors. The descriptors were shown experimentally to have a better performance than similar methods and the derived graph matching also performs well. The path descriptors are fast to compute and compare, and are usable for robust registration of large 3D images such as those coming from electron microscopy.

Acknowledgements This work was supported by the Grant Agency of the Czech Technical University in Prague, grant SGS12/190/OHK3/3T/13, the Czech Science Foundation project P202/11/0111 and the Fundação para a Ciência e Tecnologia grant SFRH/BD/77134/2011.

References

1. E. Türetken, F. Benmansour, and P. Fua, "Automated reconstruction of tree structures using path classifiers and mixed integer programming," *IEEE ICCV*, pp. 566–

573, 2012.
2. B. Zitová and J. Flusser, "Image registration methods: a survey," *Image and Vision Computing*, vol. 21, pp. 977–1000, 2003.
3. A. Can, C. V. Stewart, B. Roysam, and H. L. Tanenbaum, "A feature-based, robust, hierarchical algorithm for registering pairs of images of the curved human retina," *IEEE Trans. on Pattern Analysis and Machine Intelligence*, vol. 24, pp. 347–364, 2002.
4. E. Serradell, P. Głowacki, J. Kybic, F. Moreno-Noguer, and P. Fua, "Robust non-rigid registration of 2D and 3D graphs," *IEEE CVPR*, pp. 996–1003, 2012.
5. M. A. Pinheiro, R. Sznitman, E. Serradell, J. Kybic, F. Moreno-Noguer, and P. Fua, "Active testing search for point cloud matching," in *Information Processing in Medical Imaging*, pp. 572–583, 2013.
6. P. H. S. Torr and A. Zisserman, "MLESAC: A new robust estimator with application to estimating image geometry," *Computer Vision and Image Understanding*, vol. 78, pp. 138–156, 2000.
7. O. Chum and J. Matas, "Matching with PROSAC – progressive sample consensus," *IEEE CVPR*, pp. 220–226, 2005.
8. P. J. Besl and N. D. McKay, "A method for registration of 3-D shapes," *IEEE Trans. on Pattern Analysis and Machine Intelligence*, vol. 14, no. 2, pp. 239–256, 1992.
9. A. Myronenko and X. Song, "Point set registration: Coherent point drift," *IEEE Trans. on Pattern Analysis and Machine Intelligence*, vol. 32, no. 12, pp. 2262–2275, 2010.
10. M. Leordeanu, M. Hebert, and R. Sukthankar, "An integer projected fixed point method for graph matching and map inference," in *NIPS*, 2009.
11. M. Zaslavskiy, F. Bach, and J.-P. Vert, "A path following algorithm for the graph matching problem.," *IEEE Trans. on Pattern Analysis and Machine Intelligence*, vol. 31, no. 12, pp. 2227–42, 2009.
12. E. Serradell, F. Moreno-Noguer, J. Kybic, and P. Fua, "Robust elastic 2D/3D geometric graph matching," *SPIE Medical Imaging*, vol. 8314, no. 1, pp. 831408–831408–8, 2012.
13. R. Basri, L. Costa, D. Geiger, and D. Jacobs, "Determining the similarity of deformable shapes," *Vision Research*, vol. 38, pp. 135–143, 1998.
14. M. Frenkel and R. Basri, "Curve matching using the fast marching method," in *EMMCVPR*, pp. 35–51, 2003.
15. M. Unser, "Splines: A perfect fit for medical imaging," *Progress in Biomedical Optics and Imaging*, vol. 3, pp. 225–236, 2002.
16. T. Pajdla and L. V. Gool, "Matching of 3-D curves using semi-differential invariants," in *IEEE ICCV*, pp. 390–395, 1995.
17. M. Cho, J. Lee, and K. M. Lee, "Reweighted random walks for graph matching," in *ECCV (5)*, pp. 492–505, 2010.
18. S. Sahni, "Computationally related problems," *SIAM Journal on Computing*, vol. 3, no. 4, pp. 262–279, 1974.
19. H. W. Kuhn, "The Hungarian method for the assignment problem," *Naval Research Logistics*, vol. 2, no. 1-2, pp. 83–97, 1955.
20. K. Deng, J. Tian, J. Zheng, X. Zhang, X. Dai, and M. Xu, "Retinal fundus image registration via vascular structure graph matching," *Journal of Biomedical Imaging*, 2010.
21. A. Holtmaat, J. Randall, and M. Cane, "Optical imaging of structural and functional synaptic plasticity in vivo," *European Journal of Pharmacology*, vol. 719, no. 1–3, pp. 128 – 136, 2013.